Contemporary Mathematics
https://ojs.wiserpub.com/index.php/CM/

Research Article

Impact of Driver Anticipation on Macroscopic Traffic

Zawar H. Khan[1]*, T. Aaron Gulliver[2], Ahmed B. Altamimi[1], Wilayat Khan[1]

[1]Department of Computer Engineering, College of Computer Science and Engineering, University of Háil, Háil 55476, Saudi Arabia
[2]Department of Electrical and Computer Engineering, University of Victoria, Victoria, BC V8W 2Y2, Canada
E-mail: z.hussain@uoh.edu.sa

Received: 5 December 2025; **Revised:** 29 January 2026; **Accepted:** 6 February 2026

Abstract: Accurate characterization of heterogeneous traffic flow is essential for realistic traffic modeling. Driver anticipation in heterogeneous traffic is impacted by lateral and forward distance, vehicle size, and effective angle of vision, however most existing macroscopic models neglect these factors. Larger vehicles require greater acceleration and deceleration, while smaller vehicles maneuver more easily, and reduced visibility or limited angle of vision compromises driver response, contributing to traffic accidents. This study develops a macroscopic traffic model that explicitly incorporates driver anticipation based on effective angle of vision, distance headways, and vehicle size. An anticipation term is introduced to adjust density and velocity according to realistic traffic conditions. Further, source term based on the gravitational impact is included, to predict the velocity behavior at uphill and downhill grades. The proposed model is assesed against the classical Payne Whitham model on a circular and straight road under varying lateral headways. Results demonstrate that the proposed approach has more realistic temporal and spatial evolution of density and velocity, capturing heterogeneous flow dynamics more accurately than conventional models. These findings highlight the importance of integrating human factors, road grade, and vehicle characteristics into macroscopic traffic modeling to improve the traffic prediction accuracy.

Keywords: macroscopic model, effective angle of vision, circular road, heterogenous conditions

MSC: 76A30, 35A35, 65N06

1. Introduction

Traffic is one of the integral part of the urban life. It is one of the city communication means. This connects the residents to the facilities. Due to the incease in the cities population, vehicle traffic grows which results in increase in congestions. Due to the limited availability of land in the metropolitan cities, the roads capacity can not be increased simply and easily. Congestion mitigation is primarily managed by the accurate traffic characterization, which is one of the efficient tool to understand the traffic dynamics [1]. In the third world countries, the traffic congestion is mainly due to the heterogeneous traffic conditions. Accurate traffic characterization for heterogenous flow is an important problem [2] as the lane discipline is not followed. The traffic over all the road lanes evolves into a single traffic stream behavior with time. The driver anticipation during heterogeneous traffic depends on lateral, and forward distance headway, effective angle of vision, and vehicle size. Lateral headway is the distance between prallel vehicles, while forward distance headway is between the two following vehicles. Vehicle size is an important parameter for driver response as it affects the maneuverability.

DOI: https://doi.org/10.37256/cm.7320269347

That is, the drivers with larger vehicles are not comfortable to move and change its direction during smaller lateral and forward distance headways. Larger vehicles require greater changes in acceleration and deceleration. The smaller vehicles maneuverability is easy and comfortable. The effective angle of vision provides the information to drivers to process and take action [3]. This is important to consider the information read by the drivers and take appropriate action. Therefore, traffic characterization should consider effective angle of vision, vehicle and distance headway.

Driver presumption considers the effective angle of vision [4]. The traffic conditions include traffic control, road condition, vehicles, the roadside environment, pedestrians and animals movement. Traffic conditions can be perceived within the effective field of vision in terms of velocity [4, 5]. That is, it has an impact of the acceleration and deceleration. Obstruction in the effective angle vision region results in a compromised traffic safety [6]. For a smaller visual angle than 0.003 rad/s, the traffic conditions are not perceivable [4]. The road environment depends on the illumination conditions such as day, night, rain, foggy, ice or snow. This also includes sources of reflections, and glare [7]. To account for the visual information, the time to collision is introduced in driver assist technologies [8–11]. Effective angle of vision impacted by illumination results in traffic accidents. For example, under the reduced visibility during fog $38,700$ accidents occur in the US annually. Consequently, $16,300$ injuries and 600 fatalities occur anualy due to the reduced visibility [12]. That is, the information perception is compromised, which results in these accidents [13]. Reduced visibility impacts angle of vision which reduces driver ability of anticipation [14]. The experienced drivers accidents rate is smaller than the new drivers [15]. The cues for obstruction in the effective angle of vision are insufficient, and is a typical cause of accidents [16]. Most traffic models do not consider effective angle of vision. Therfore, it is significant to consider its impact on traffic chracterization.

Vehicle size impacts the traffic flow and safety. From 2012 to 2021, large vehicles hold three fourth share of the market. In 2012, 12 people were killed in the road accidents, while in 2021, this number is increased to 14 people for every $100,000$ vehicles. The impact of large vehicles at the same speed in the traffic accident is larger than with smaller vehicles. The impact force of a truck at 72.42 km/h is 470 kN, while for a sedan it is 320 KN. Larger vehicles traveling at speeds above 32.19 km/h exert an exponentially greater impact in accidents compared to smaller vehicles, such as sedans. When an SUV hits a pedestrian at speeds of 64 km/h or higher, the collision is fatal. In contrast, when a standard passenger car hits a pedestrian at the same speed, the chances of fatality is 50% [17]. Distance headway is one of the safety factors on the road. Maintaining smaller headway causes tail and sideways crashes and accounts for one third of road accidents [18]. For shorter distance headways, drivers have less chance of braking and lane change [19]. Thus headway is a safety factor in determining the accidents. Driver anticipation, a key determinant of traffic flow variability, is strongly influenced by both lateral and forward distance headways. In heterogeneous traffic, vehicles continuously adapt their speeds in response to these distances. Consequently, a realistic characterization of traffic must incorporate the coupled effects of lateral and forward headways along with vehicle size, as these factors jointly govern driver response and overall flow stability.

Most of the common traffic characterization are macroscopic, mesoscopic and microscopic [20]. Macroscopic models are based on average density, velocity, and flow [21]. These models provides the collective traffic behavior. Macroscopic systems are deterministic models and are governed by partial differential equations. Microscopic models characterizes the individual vehicles behavior [22]. These models consider lane changing, braking, acceleration and following behavior. Mesoscopic models share the properties of both the microscopic and macroscopic models. These models consider the vehicles platoons and characterizes the statistical traffic behavior. Macroscopic models are computational efficient models and are considered in this paper.

The Lighthill, Whitham, and Richards (LWR) model [23, 24] is a deterministic macroscopic model, and is

$$\rho_t + \rho(v(\rho))_x = 0, \tag{1}$$

ρ denotes density, while $v(\rho)$ denotes the equilibrium velocity distribution [25]. The subscript t characterizes temporal evolution, while the subscript x is the spatial evolution. This model characterizes traffic changes. LWR model can characterize road networks [26, 27]. A traffic change is instantaneous which is inappropriate [28, 29], and has high computational demand [30]. $v(\rho)$ is desired velocity to achieve the equilibrium flow. This velocity increases as the

density decreases [31, 32]. Different velocity distributions are characterized [33, 34], but for simplicity, the Greenshields distribution [35] is considered. That is

$$v(\rho) = v_m \left(1 - \frac{\rho}{\rho_m}\right), \tag{2}$$

v_m denotes the maximum velocity and ρ_m denotes the maximum density. In this paper, (2) is employed.

Payne and Whitham (PW) model improved the LWR model by considering traffic acceleration and driver anticipation [36, 37]. The driver anticipation is based on a constant C_0 [35], and is uniform for all traffic conditions [36, 38]. This results in large changes in velocity at larger density changes, which is impractical. To address sudden velocity changes, the PW model was refined in [39]. However, this model ignores heterogeneous traffic behavior [40], and has limitations at traffic merging locations [41]. A driver has individual traits, psychological perspectives, and experience [42]. And leads to differences in drivers perception, and taking decisions under the same road traffic conditions resulting in distinct driving behaviors. The driver behavior is ignored by the macroscopic PW type models, while the changes in traffic arises from the aggregated individual drivers behavior. One of the example is the phantom traffic jam, which typically arises due to the delayed driver response [43]. Additional extensions included the introduction of driver reaction time in [44], and anticipation based on density effects in [45, 46]. However, these models fail to capture traffic dynamics in heterogeneous traffic conditions. These models did not consider traffic physics explicitly. PW type models are improved by condering diffusion to avoid the large velocity changes but this is unrealistic [47, 48]. In [49], the Payne Whitham model was improved by substituting the density gradient with a velocity gradient such that changes in traffic behavior are at or below the average speed. However, some of the vehicles are at higher speed than the average. So the traditional models approach for the changes occuring below and above the average speed are accurate and requires to be based on the realistic traffic physics.

The realistic traffic chracterization has been ignored during heterogeneous flow. Further, most of the existing models in the literature assume uniform driver anticipation and as well as ideal traffic conditions. The deterministic models oversimplify the traffic conditions and ignore the realistic traffic changes [50]. The human factors such as effective angle of vision, safety factors such as lateral and forward distance headways and the vehicle size are ignored. Some of the microscopic models employ human behavior, but are computationaly more complex. Therefore, a macroscopic (determinsitic) model is developed which integrates the effective angle of vision, distance headways and the vehicle size. That is, a model is proposed which can realistically characterize heterogeneous flow. In particular, driver anticipation is developed for the proposed model. It adjusts density and velocity according to the realistic parameters incorporated which more accurately characterizes traffic evolution. The PW and proposed modesl are evaluated on a $3,000$ m circular and straight road. The results illustrate that the density and velocity temporal and spatial evolution are more realistic than the PW model.

More accurate and reliable traffic prediction is crucial for capturing the real world traffic dynamics. The objective is to develop a macroscopic model that integrates the effects of angle of vision, distance headways, and vehicle size on driver behavior. The specific goal is to analyze traffic velocity, density, and driver anticipation in relation to lateral distance headway. Driver behavior, and thus traffic density and flow, are significantly influenced by the angle of vision, vehicle size, and lateral and forward distance headways. These factors are not well captured in the existing macroscopic models. Incorporating these factors into the proposed traffic model can realistically characterize traffic evolution. That is the changes in velocity are dependent on density, and should stay within the employed range. Further, the driver anticipation is in proportionate with the traffic changes.

The rest of this paper is organized as follows. Section 2 presents the proposed macroscopic traffic model, and the hyperbolicity is evaluated. The string stability is analyzed in Section 3. Section 4 provides performance results for both the models over a circular and straight road. Finally Section 5 concludes this paper.

2. Traffic models

The PW model is expressed as

$$\rho_t + \rho(v(\rho))_x = 0,$$

$$(\rho v)_t + \left(\frac{(\rho v)^2}{\rho} + C_0^2\rho\right)_x = \rho\left(\frac{v(\rho) - v}{\tau}\right), \tag{3}$$

where $C_0^2\rho$ represents driver anticipation. Assuming anticipation to be a constant leads to unrealistic behavior, particularly under large density variations. Drivers typically respond more strongly in high density traffic and less in low density conditions [51]. The relaxation term $\rho\left(\frac{v(\rho) - v}{\tau}\right)$ characterizes adaptation toward equilibrium conditions, with the relaxation time τ governing the alignment rate. A larger τ corresponds to slower adjustment. A variable anticipation based on realistic parameters is required to respond appropriately to changes ahead. The PW model neglects the changes in velocity, effective angle of vision, forward and lateral distance headway. The effective angle of vision is the angular range of an eye within which a driver can perceive and react to vehicles ahead, road signs, and hazards without moving their head. A driver only relies on eye movement. This is smaller than the total field of vision, and typically is 120° horizontally and 50° vertically. Within this range, the visually acuity is sufficient to safely perceive and react to conditions ahead. Outside this range, the objects are visible but not accurately recognizable by a driver to react. The effective angle of vision in traffic characterization describes the road environment which a driver can realistically pereceive and react. The effective vision angle is dependent on the width of a vehicle and its distance from the driver. The PW model irrespective of the traffic conditions adapts to equilibrium uniformly, which is unrealistic and inappropriate. In this section, this limitation by is addresed by introducing a deterministic model based on effective vision angle, forward and lateral distance headway to affectively capture more realistic driver behavior.

In heterogeneous traffic, flow behavior is strongly impacted by both lateral and forward distance headways. A larger lateral and longitudinal headway, results in smoother and smaller fluctuations in traffic. Vehicles have sufficient distance to adapt with smaller changes. Conversely, at smaller headways, interactions between vehicles are more intense. The traffic changes are more predictabile but this causes a large traffic instabilities. Larger vehicle interactions cause stop and go traffic, and are one of the characteristic features of traffic congestion. The changes in vehicle speed adaptation play a key role in traffc behavior. When a driver adjust the vehicle speed more slowly (slow alignment), then the traffic changes strongly propagate through the traffic stream. This amplifies traffic changes. While, faster alignment to the forward traffic leads to a more stable traffic flow. The changes in flow has the tendency to reduce with time. Additionally, vehicle length also impacts heterogeneous traffic. Larger vehicles have lower maneuverability. Typically larger headway is maintained between larger vehicles. Traffic alignment is slower, which results in larger changes. Whereas, smaller vehicles maintain smaller distance headway and has high maneuverability. Therefore aligns more easily and quickly which results in smaller changes. The integrated effect of distance headways, changes in speed and vehicle size critically impacts the heterogeneous traffic stability and variability. Therefore, the driver anticipation should consider the velocity changes, vehicle length, lateral and forward distance headways. Since the individual driver behavior impacts the macroscopic traffic evolution [52], then C_0 can be characterized as

$$\frac{\delta v \mu \eta}{f^2}, \tag{4}$$

where $\delta v = v_m - v_l$, v_l is the leading vehicle velocity and v_m is the maximum velocity. μ is the intensity of forward distance headway and characterized as $\frac{1}{d_n}$, where d_n is the forward distance headway. η is the vehicle length and f is the lateral

distance headway. Further, driver anticipation depends on the effective angle of vision, that is it provides the driver ability to process road information. The effective angle of vision is

$$\tan^{-1}\left(\frac{w}{D}\right), \tag{5}$$

while w is the road width and D is the forward readable distance. Then C_0 can be characterized as

$$C_0 = \frac{\delta v \mu \eta}{f^2}\tan^{-1}\left(\frac{w}{D}\right). \tag{6}$$

Therefore, substituting (6) in (3) gives

$$\begin{aligned}
&\rho_t + (\rho v(\rho))_x = 0,\\
&(\rho v)_t + \left(\frac{(\rho v)^2}{\rho} + \left(\frac{\delta v \mu \eta}{f^2}\tan^{-1}\left(\frac{w}{D}\right)\right)^2 \rho\right)_x = \rho\left(\frac{v(\rho)-v}{\tau}\right).
\end{aligned} \tag{7}$$

Equation (7) describes traffic behavior in heterogenous conditions by considering changes in velocity, lateral and forward distance headways, vehicle length and effective angle of vision. $\frac{\delta v \mu \eta}{f^2}\tan^{-1}\left(\frac{w}{D}\right)\rho$ is the realistic driver anticipation for vehicles alignment in heterogeneous conditions. The driver anticipation is $C_0^2\rho$ in the PW model (3), and vehicles align with a uniform response at the rate C_0. This is unrealistic and inappropriate, and ignores the real world traffic dynamics. The proposed system first equation (7) is identical to the PW model (3).

The traffic behavior is impacted by the road geometry, that is, particularly longitudinal gradients has a critical role in density and velocity evolution. The longitudnal grades influence vehicles acceleration/deceleration, fuel consumption, and traffic stability. The additional resistive forces imposed due to the uphill gradient reduces the vehicles speed which reduces the road capacity, and results in increased congestion. Conversely, downhill gradients assisting in vehicle motion increases the speed. Therefore, the employment of logitudnal grades effect in the macroscopic traffic flow models is significant to accurately characterize traffic behavior, that is to realistically predict congestion, energy consumption and emission impacts under different road geometries. That is, the acceleration/deceleration due the longitudnal can be characterized as

$$\rho g \vartheta, \tag{8}$$

where g is the gravitation acceleration and ϑ is the road grade. This grad varies from 1% to 12% for access roads. Substiting (8) in source term, (7) becomes

$$\begin{aligned}
&\rho_t + (\rho v(\rho))_x = 0,\\
&(\rho v)_t + \left(\frac{(\rho v)^2}{\rho} + \left(\frac{\delta v \mu \eta}{f^2}\tan^{-1}\left(\frac{w}{D}\right)\right)^2 \rho\right)_x = \rho\left(\frac{v(\rho)-v}{\tau} \pm g\vartheta\right).
\end{aligned} \tag{9}$$

The acceleration in (9) due to the longitudnal grade at downhill is $+\rho g\vartheta$, while the deceleration at uphill is -$\rho g\vartheta$.

It is significant that a traffic model be hyperbolic to ensure well posed and predictable solution. The changes in the traffic systems are smoother and do not grow at abrupt changes in density [53]. A hyperbolic traffic system has a valid solution such that eigenvalues are distinct and real [46]. Therefore, proposed and the traditional PW models eigenvalues are analyzed. The PW and proposed models can be represented as

$$\beta_t + f(\beta)_x = S(\beta), \tag{10}$$

whereas x and t denote the spatial temporal changes in traffic. The PW model traffic data variables vector is $\beta = \begin{pmatrix} \rho \\ \rho v \end{pmatrix}$ [54], while the vector of functions is $f(\beta) = \begin{pmatrix} \rho v \\ \frac{(\rho v)^2}{\rho} + {C_0}^2 \rho \end{pmatrix}$, and source vector is $S(\beta) = \begin{pmatrix} 0 \\ \rho \frac{v(\rho) - v}{\tau} \end{pmatrix}$ are obtained from (3).

$\beta = \begin{pmatrix} \rho \\ \rho v \end{pmatrix}$ is the proposed model variable vector obtained from (7), while

$$f(\beta) = \begin{pmatrix} \rho v \\ \frac{(\rho v)^2}{\rho} + \left(\frac{\delta v \mu \eta}{f^2} \tan^{-1}\left(\frac{w}{D}\right) \right)^2 \rho \end{pmatrix}$$

is the functions vector. $S(\beta) = \begin{pmatrix} 0 \\ \rho \frac{v(\rho) - v}{\tau} \end{pmatrix}$ is the source vector.

$$\begin{aligned} \lambda_1 &= v + C_0, \\ \lambda_2 &= v - C_0. \end{aligned} \tag{11}$$

The eigenvalues (11) of the PW model are distinct and real and ensures a well posed solution (11) . The eigenvalues confirm that PW model is hyperbolic. λ_1 characterizes the free flow, while λ_2 characterizes traffic during congestion with a uniform constant C_0. This C_0 is not based on the traffic physically but rather is a fitting parameter. Consequently, the traffic characterization is unrealistic during congestion.

The proposed model eigenvalues are

$$\lambda_1 = v + \frac{\delta v \mu \eta}{f^2} \tan^{-1}\left(\frac{w}{D}\right), \quad \lambda_2 = v - \frac{\delta v \mu \eta}{f^2} \tan^{-1}\left(\frac{w}{D}\right). \tag{12}$$

The eigenvalues (12) are distinct and real, that is, the solution of the proposed model is well posed. This ensures that the proposed model is hyperbolic. λ_1 in (12) characterizes the free flow conditions, while λ_2 chracterizes traffic changes during congestion. The traffic changes in both the eigenvalues λ_1 and λ_2 of the proposed are impacted by effective angle of vision, vehicle size, lateral and forward distance headways.

3. The proposed model string stability

String stability gurantees that small changes in the traffic do not grow in the traffic behavior and consequently, traffic has the tendency of smooth flow. Whereas in an unstable traffic congestion forms easily as changes amplify with time [55]. Unstable traffic exhibits disproportionate behavior at small changes. Stop and go traffic behavior is exhibited which is a behavior at large changes. This compromises traffic safety as large accerleration and deceleration occur. This increases the traffic accidents chances, and ultimately the driver comfort is reduced. Thus, the PW and proposed models string stability is analyzed.

The equilibrium velocity distribution for initial density ρ_0 is $v_0 = v(\rho_0)$. Then the flow q_0 is $\rho_0 v(\rho_0)$, whereas the gradient of equilibrium velocity distribution is $v'(\rho_0)$. The temporal and spatial density and velocity for small changes in density $\delta\rho$ and velocity δv are

$$\rho(x,\, t) = \rho_0 + \delta\rho, \quad v(x,\, t) = v_0 + \delta v,$$

ζ denotes the frequency of oscillation over the time, and is measured in rad/s. It characterizes the traffic changes temporally, and is $\zeta = 2\pi f$, and f denotes frequency of traffic changes per unit time. k denotes the frequency of traffic changes over the distance, and is measured in rad/m. It characterizes traffic oscillations per unit distance, and is $k = \dfrac{2\pi}{\lambda}$. The traffic oscillations are repeated over λ, and is the distance period. For traffic stablility, the velocity and density changes do not grow over λ with k for ζ, and decays with the distance and time evolution. The small traffic density and flow changes in vector form are

$$\mathbf{Z} = \begin{pmatrix} \delta\rho \\ \delta q \end{pmatrix}. \tag{13}$$

The changes in flow are $\delta q = \rho_0\, \delta v + v_0\, \delta\rho$. The proposed model in the form of density and flow is

$$\begin{aligned} &\rho_t + (q)_x = 0, \\ &(q)_t + \left(\frac{(q)^2}{\rho} + \varepsilon^2\rho\right)_x = \rho\, \frac{v(\rho) - \dfrac{q}{\rho}}{\tau}. \end{aligned} \tag{14}$$

For simplicity, let ε denotes $\dfrac{\delta v \mu \eta}{f^2} \tan^{-1}\left(\dfrac{w}{D}\right)$ in the proposed model. The linearized system for the deterministic proposed model is

$$\mathbf{Z}_t + \alpha\, \mathbf{Z}_x = A\, \mathbf{Z}. \tag{15}$$

Let the amplitude vector of the traffic changes be $\hat{\mathbf{Z}}$, then

$$\mathbf{Z}(x,\, t) = \hat{\mathbf{Z}}\, e^{i(kx - \zeta t)}. \tag{16}$$

Then the temporal change in $\mathbf{Z}(x,\ t)$ is

$$\mathbf{Z}_t = -i\zeta\,\hat{\mathbf{Z}}\,e^{i(kx-\zeta t)}, \tag{17}$$

while the spatial change in $\mathbf{Z}(x,\ t)$ is

$$\mathbf{Z}_x = ik\,\hat{\mathbf{Z}}\,e^{i(kx-\zeta t)}. \tag{18}$$

From (16), (17) and (15), (18) is obtained as

$$\left(-i\,\zeta\,I + i\,k\,\alpha - A\right)\hat{\mathbf{Z}} = \mathbf{0}, \tag{19}$$

while $e^{i(kx-\zeta t)}$ is factored out. Then,

$$\det\left(-i\,\zeta\,I + i\,k\,\alpha - A\right) = 0, \tag{20}$$

$\zeta = \zeta(k)$ is obtained from (20), as a function of k .

The Jacobian for small changes at equilibrium $(\rho_0,\ q_0)$ is

$$\alpha = \begin{pmatrix} 0 & 1 \\ -v_0^2 + \varepsilon^2 & 2\,v_0 \end{pmatrix}, \tag{21}$$

while A for source is

$$A = \begin{pmatrix} 0 & 0 \\ \dfrac{\rho_0\,v'(\rho_0)}{\tau} & -\dfrac{1}{\tau} \end{pmatrix}. \tag{22}$$

The quadratic equation for ζ is obtained from α and ω by substituting in (20) as

$$\zeta^2 - \left(2v_0k - \frac{i}{\tau}\right)\zeta - k^2\left(\varepsilon^2 - v_0^2\right) + ik\frac{\rho_0\,v'(\rho_0)}{\tau} = 0. \tag{23}$$

The solution of (23) gives $\zeta_{1,\,2}(k)$ as a function of k, and in simplified form is

$$\zeta_{1,\,2}(k) = v_0\,k\ -\ \frac{i}{2\tau}\ \pm\ \sqrt{k^2\varepsilon^2 -\ \frac{i\,k\,(v_0 + \rho_0\,v'(\rho_0))}{\tau} - \frac{1}{4\tau^2}}, \tag{24}$$

ε is substituted as $\frac{\delta v \mu \eta}{f^2} \tan^{-1}\left(\frac{w}{D}\right)$ in (24), which gives $\zeta_{1,\,2}(k)$ as

$$\zeta_{1,\,2}(k) = v_0 k - \frac{i}{2\tau} \pm \sqrt{k^2 \left(\frac{\delta v \mu \eta}{f^2} \tan^{-1}\left(\frac{w}{D}\right)\right)^2 - \frac{ik(v_0 + \rho_0 v'(\rho_0))}{\tau} - \frac{1}{4\tau^2}}\,. \tag{25}$$

The deterministic proposed traffic system is string stable for $\Im(\zeta(k)) < 0$, in other words the traffic changes reduce temporally.

$$\forall k > 0: \quad \Im\big(\zeta_1(k)\big) < 0 \quad \text{and} \quad \Im\big(\zeta_2(k)\big) < 0. \tag{26}$$

The anticipation depends on the effective angle of vision, vehicle size, forward and lateral distance heaways. Equation (26) ensures upper limit on τ related to anticipation ε and the change in equilibrium velocity $v'(\rho_0)$. That is changes in traffic dissipate with time over the distance. Conversely, for $\Im(\zeta(k)) > 0$, the changes grow and causes a congested traffic.

The phase speed is $S_{1,\,2} = \frac{\Re(\zeta(k)_{1,\,2})}{k}$ characterizes the speed of the peak of smaller and larger changes in traffic over the distance. For $S > 0$, the changes in speed are along the traffic direction, while for $S < 0$, the changes travel backwards. This is the speed of the stop and go traffic changes. $|c|$ indicates rate of changes that travel in the traffic.

Equation (25) is implemented in MATLAB for string stability analysis with the parameters as $\mu = 1$ m, $\eta = 5$ m, $\tau = 4$ s, $v_m = 20$ m/s, $w = 36$ m, $\rho_0 = 0.5$ and $D = 100$ m. The traffic achieves the desirable velocity as Greenshields distribution. Figure 1 illustrates $\zeta_{1,\,2}(k)$ from (25) which are plotted over k. It is observed that $\Im\{\zeta_{1,\,2}(k)\}$ is less than 0 for all values of k. Therefore the proposed system (7) gives string behavior. That is, the changes in traffic dissipate over time.

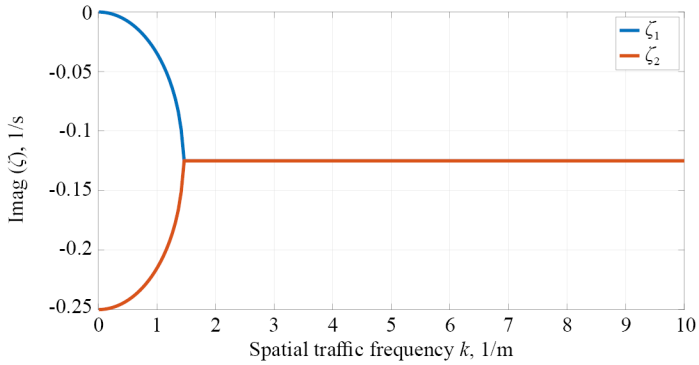

Figure 1. The imaginary part of ω over the spatial frequency k

It is observed in the Figure 2 that $S_{1,\,2}$ is above 0 for all values of k, which indicates that the traffic changes travel along the traffic direction. The traffic has then tendency of reduced traffic changes and do not predict congested traffic as $S_{1,\,2}$ are positive.

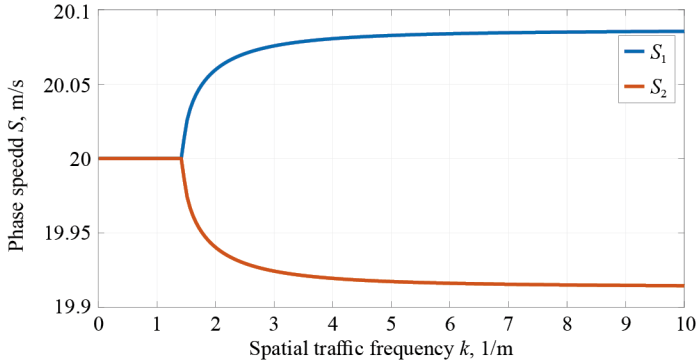

Figure 2. The phase speed $S_{1,\,2}$ over the spatial frequency k

4. Performance results

4.1 *First Order Centered (FORCE) scheme*

Implementation of the proposed model and the PW model in MATLAB employs the FORCE scheme [56], which accurately handles sharp gradients and abrupt changes in traffic flow. The FORCE scheme is widely adopted in traffic modeling [57] due to its balance between accuracy and computational cost. The Richtmyer and Lax Friedrichs methods combination provides a robust approximation for the PW types system with lower computational cost than the Roe scheme [57]. Consider the conserved of the PW and proposed models from (10) as

$$\partial_t \beta(x,\,t) + \partial_x F(\beta(x,\,t)) = 0, \tag{27}$$

where β is the vector of conserved variables ρ and ρv. Where $F(\beta)$ is the flux vector. Let β_i^n denote the cell-averaged solution in cell i at time t^n, then

$$\beta_i^{n+1} = \beta_i^n - \frac{\Delta t}{\Delta x}\left(\widehat{F}_{i+\frac{1}{2}}^n - \widehat{F}_{i-\frac{1}{2}}^n\right), \tag{28}$$

where $\widehat{F}_{i+\frac{1}{2}}$ is a numerical flux. The FORCE flux is the arithmetic average of the Lax-Friedrichs (LF) flux and the Richtmyer (RI) flux, that is

$$\widehat{F}_{i+\frac{1}{2}}^{\mathrm{FORCE}} = \frac{1}{2}\left(\widehat{F}_{i+\frac{1}{2}}^{\mathrm{LF}} + \widehat{F}_{i+\frac{1}{2}}^{\mathrm{RI}}\right). \tag{29}$$

The Lax-Friedrichs flux is

$$\widehat{F}_{i+\frac{1}{2}}^{\mathrm{LF}} = \frac{1}{2}\left(F(\beta_i^n) + F(\beta_{i+1}^n)\right) - \frac{1}{2}\frac{\Delta x}{\Delta t}\left(\beta_{i+1}^n - \beta_i^n\right), \tag{30}$$

and the Richtmyer flux is iterated as

$$\beta_{i+\frac{1}{2}}^{\mathrm{RI}} = \frac{1}{2}\left(\beta_i^n + \beta_{i+1}^n\right) - \frac{1}{2}\frac{\Delta t}{\Delta x}\left(F(\beta_{i+1}^n) - F(\beta_i^n)\right), \tag{31}$$

and the corresponding Richtmyer flux is

$$\widehat{F}_{i+\frac{1}{2}}^{\mathrm{RI}} = F\left(\beta_{i+\frac{1}{2}}^{\mathrm{RI}}\right). \tag{32}$$

To ensure the numerical iteration stability, the Courant-Friedrichs-Lewy (CFL) condition is employed, that is the time step Δt is chosen as

$$\Delta t \leq \mathrm{CFL}\,\frac{\Delta x}{\max_i \left|\lambda_1\left(\dfrac{\partial F}{\partial \beta}(\beta_i^n)\right)\right|}. \tag{33}$$

Peak to peak velocity is a stability metric which quantifies the traffic oscillations amplitude. Smaller values of peak to peak velocity indicate reduced congestion, improved traffic smoothness, and enhanced energy efficiency. In this paper, peak to peak velocity are presented for performance analysis. Considering a discretized traffic system, then velocity and density are

$$v(x_i,\, t_n),\ \rho(x_i,\, t_n), \quad i = 1,\, \ldots,\, N,\ n = 1,\, \ldots,\, T, \tag{34}$$

and the peak to peak velocity at ith road segment is then given as

$$v_{\mathrm{pp}}(x_i) = \max_{1\leq n\leq T} v(x_i,\, t_n) - \min_{1\leq n\leq T} v(x_i,\, t_n), \tag{35}$$

while the average peak to peak velocity is

$$\overline{v_{\mathrm{pp}}} = \frac{1}{N}\sum_i v_{\mathrm{pp}(x_i)}.$$

4.2 *Simulation results*

4.2.1 *Traffic over a circular road*

A circular road of 3,000 m is used to evaluate the models performance. The simulation parameters are provided in Table 1. The numerical stability is ensured by imposing the CFL condition [58]. For both models, the spatial and temporal discretizations are chosen as $\Delta x = 10$ m and $\Delta t = 0.01$ s, respectively, and all simulations are implemented in Matlab R2019b. Each simulation runs for 100 s to achieve the equilibrium velocity distribution defined in (2). The vehicle length is fixed at 5 m [59]. The maximum density ρ_m is 1, while the forward headway under congested conditions is $\dfrac{1}{\rho_m} = 1$ m [52]. The road width is 36 m, while the forward readable distance is 100 m [60]. Two lateral headways are considered that is 1.3 m and 2.2 m [61], following empirical studies on lane changing behavior and vehicle spacing in heterogeneous traffic [62]. v_m is 22 m/s, and v_l is 18 m/s, while the relaxation time is $\tau = 4$ s [63, 64].

Table 1. Simulation parameters for the proposed and PW traffic models

Description	Value
Total time of simulation	100 s
Circular road length	3,000 m
Maximum velocity v_m	22 m/s
Readable forward distance D	100 m
Width of the road w	36 m
Following vehicle velocity v_l	18 m/s
Time step Δt	0.01 s
Road step Δx	10 m
Relaxation time τ	4 s
Vehicle length η	5 m
Lateral distance headway f	1.3 m, 2.2 m
Forward distance headway μ	1 m
Velocity distribution	Greenshields, (2)
Maximum normalized density ρ_m	1
Speed constant C_0	25 m/s

The density at $t = 0$ is

$$\rho_0 = \begin{cases} 0.02, & \text{for } x \leq 500, \\ 0.3, & \text{for } 500 < x \leq 1,200, \\ 0.02, & \text{for } 1,200 < x \leq 1,700, \\ 0.3, & \text{for } 1,700 < x \leq 2,500, \\ 0.01, & \text{for } x \leq 3,000. \end{cases} \tag{36}$$

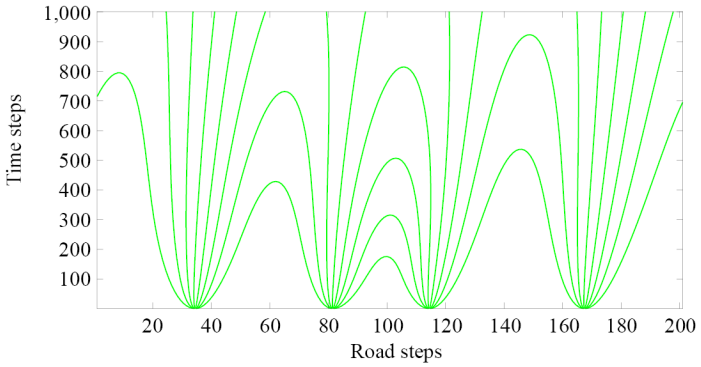

Figure 3. The proposed model density contours with wavefronts over 200 road steps, while the lateral distance headway is 1.3 m

As C_0 in the Payne-Whitham model varies between 2.4 m/s and 57 m/s. In alignment with this range, a value of $C_0 = 25$ m/s is selected for use in this paper.

Figure 3 presents the spatio temporal evolution of traffic density using contour lines over 200 road steps and 1,000 time steps. The contour wavefronts illustrate the propagation of density waves, where closely spaced lines correspond to sharp gradients (shock waves) and wider spacing reflects smoother variations (rarefaction waves). At the initial stages close to 1st time step, the density fluctuations appear sharper and more localized, while over time these chages spread and evolve into smoother wavefronts. The recurring arch-like patterns indicate the formation and dissipation of stop and go traffic, highlighting the proposed model ability to capture both shock formation and rarefaction dynamics in traffic flow.

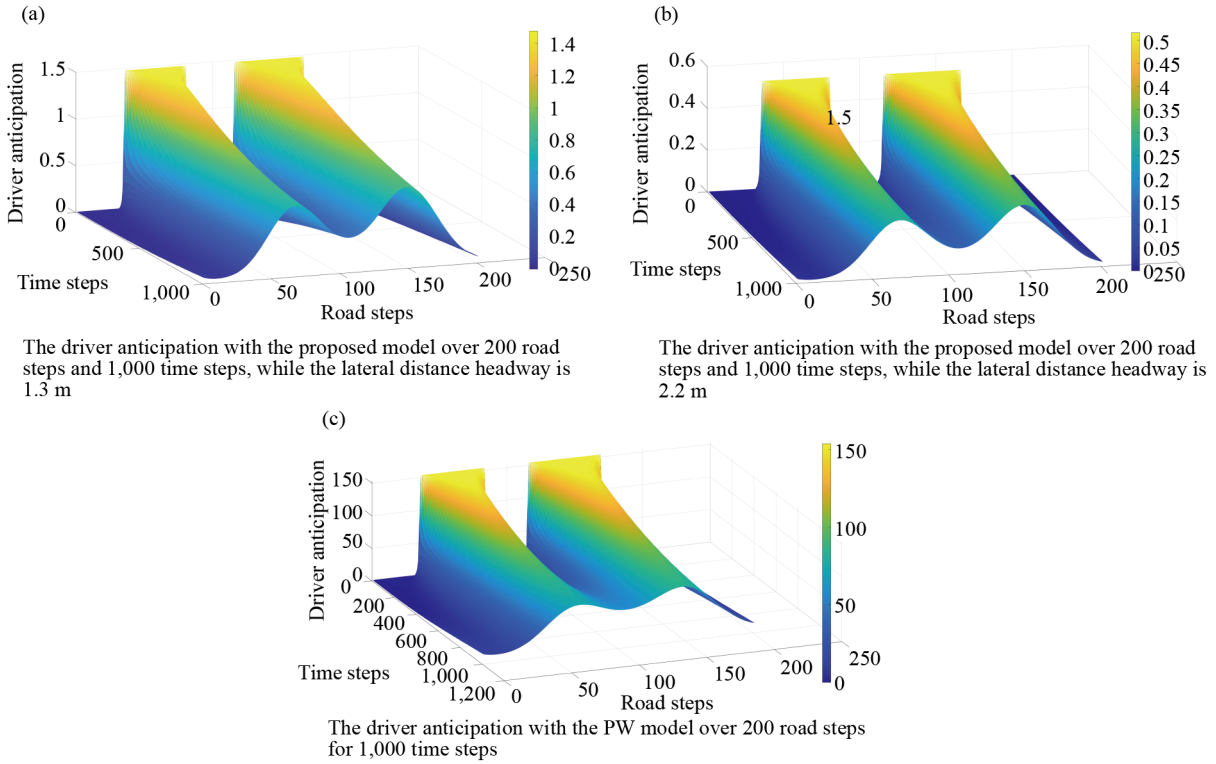

The driver anticipation with the proposed model over 200 road steps and 1,000 time steps, while the lateral distance headway is 1.3 m

The driver anticipation with the proposed model over 200 road steps and 1,000 time steps, while the lateral distance headway is 2.2 m

The driver anticipation with the PW model over 200 road steps for 1,000 time steps

Figure 4. Comparison of driver anticipation on a circular 3,000 m road: proposed model with lateral headway of (a) 1.3 m, (b) 2.2 m, and (c) PW model

Figure 4a demonstrates the driver anticipation behavior with the proposed model over 200 road steps and 1,000 time steps with a lateral distance headway of 1.3 m. At 1st time step, the driver anticipation is 1.48 at 57th road step, which reduces to 0.65 at 3,000th time step. The driver anticipation at 1st time step is 1.48 at 144th road step, which reduces to 0.85 at 3,000th time step. At 1,000th time step, the maximum driver anticipation is 0.87, while the minimum is 0.054. Figure 4b demonstrates the driver anticipation behavior with the proposed model over 200 road steps and 1,000 time steps with a lateral distance headway of 2.2 m. At 1st time step, the driver anticipation is 0.52 at 57th road step, which reduces to 0.24 at 3,000th time step. The driver anticipation at 1st time step is 0.52 at 144th road step, which reduces to 0.31 at 3,000th time step. At 1,000th time step, the maximum driver anticipation is 0.32, while the minimum is 0.014. Figures 4a and 4b show that with smaller lateral headway, the driver anticipation is larger while with a larger lateral distance headway, the driver anticipation is smaller. That is, the vehicles are in proximity with a smaller lateral distance headway, and has larger chances of collision. The driver alertness is high and as shown in the results, stronger driver anticipation occurs. Conversely, a larger lateral headway gives more comfort to driver as the collision risk is reduced and results in weaker driver anticipation. Consequently, smaller lateral distance headway increases driver anticipation, which enhances the traffic

stability and reduces the velocity changes. whereas the larger lateral distance headway reduces anticipation and results in larger traffic oscilations.

Figure 4c illustrates the spatial and temporal evolution of driver anticipation using the PW model over 200 road steps and 1,000 time steps. At the 2nd time step, the driver anticipation at the 54th road step is 153.8, which decreases to 58.03 by the 1,000th time step. Similarly, at the 146th time step, the anticipation remains 153.8 but later reduces to 83.37. Overall, the PW model yields higher anticipation values compared to the proposed model (Figures 4a and 4b), leading to higher changes in traffic flow.

Figures 5a and 5b present the density evolution obtained with the proposed model over a 3,000 m road segment across 1,000 time steps, considering lateral headways of 1.3 m and 2.2 m, respectively. In both cases, the density is within the specified range of 0 to 1. The sharp variations observed at the initial time step gradually evolve into smoother fluctuations by the 1,000th time step.

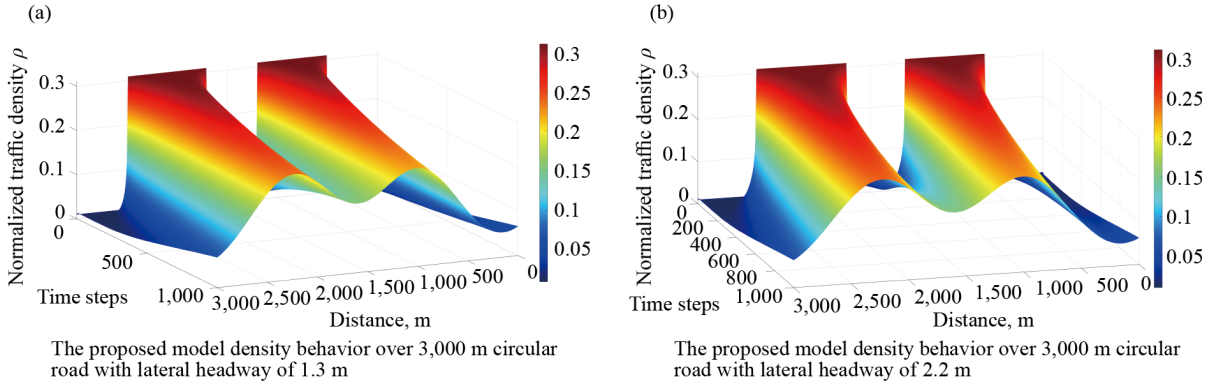

Figure 5. Comparison of traffic density behavior on a circular 3,000 m road: proposed model with lateral distance headway (a) 1.3 m and (b) 2.2 m

Figures 6a and 6b illustrate the corresponding velocity profiles for the same simulation conditions. Consistent with Figures 5a and 5b, the results show higher traffic velocity at lower densities and reduced velocity at higher densities, thereby validating the accuracy of the proposed model. Moreover, the velocity remains within the specified range of 0 to 22 m/s, further confirming the reliability of the model predictions. The minimum velocity 16.43 m/s at 1,000th time step with lateral distance headway of 1.3 m occurs at 2,250 m as shown in Figure 6a. While the maximum 20.10 m/s at 1,000th time step occurs at 150 m. The minimum velocity 16.33 m/s at 1,000th time step with lateral distance headway of 2.2 m occurs at 2,130 m as shown in Figure 6b. While the maximum 20.85 m/s at 1,000th time step occurs at 1 m and 3,000 m.

Figure 6c presents the traffic velocity obtained with the PW model over 200 road steps and 1,000 time steps. The maximum velocity of 31.73 m/s occurs at the 189th road step and the 292nd time step, which is unrealistic since it exceeds the upper limit of 22 m/s. The spatial and temporal velocity profiles also exhibit stronger oscillations compared to the proposed model, leading to the emergence of stop and go traffic.

The velocity versus density phase diagram of the PW is shown in Figure 7a. It is demonstrated that the PW model produces wide oscillatory trajectories, and nonphysical states that is velocitiy exceed the maxium 22 m/s. The scattered loops over wider range of density indicate stop and go traffic. This reflects that instability is induced by excessive driver anticipation, which highlights the PW model limitations. It is noted that the velocity increases largely beyond the employed range at abrupt chnages which does not resemble with the fundamental diagram. That is, the velocity must decrease as the density increases at the abrupt changes, and therefore, the PW model results are inappropriate and impractical. ghlighting the limitations of the PW formulation.

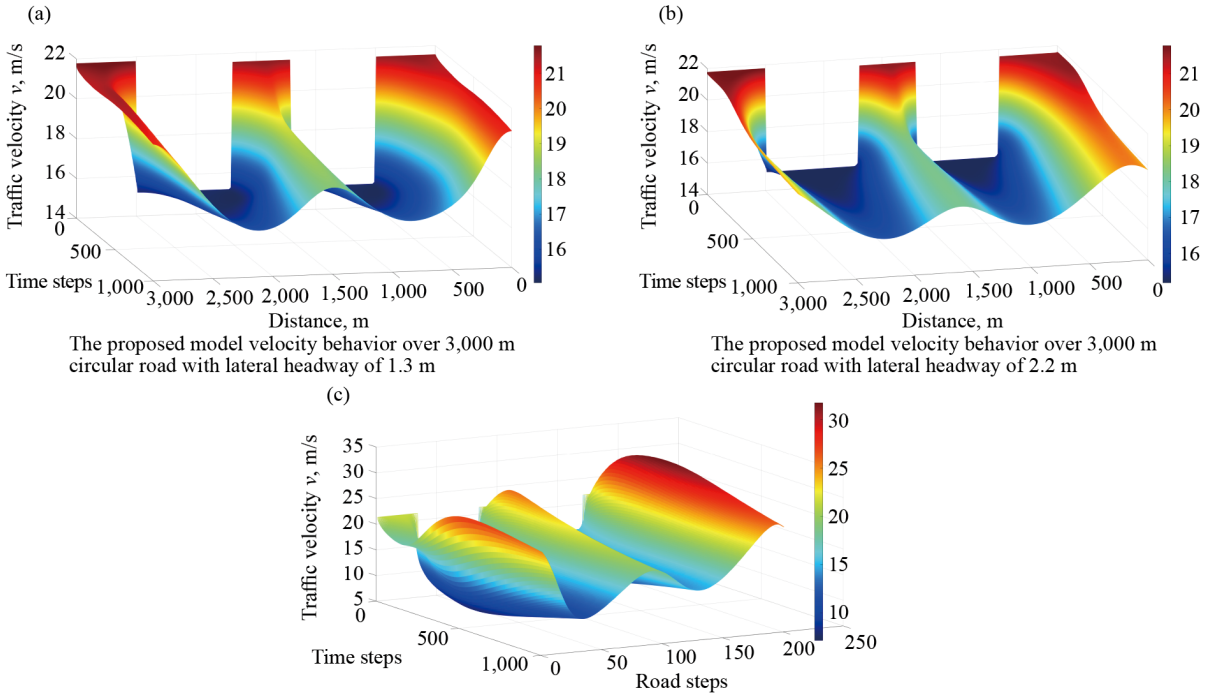

The proposed model velocity behavior over 3,000 m circular road with lateral headway of 1.3 m

The proposed model velocity behavior over 3,000 m circular road with lateral headway of 2.2 m

The PW model velocity behavior over 200 road steps for 1,000 time steps

Figure 6. Comparison of traffic velocity behavior on a circular 3,000 m road: proposed model with lateral headway of (a) 1.3 m, (b) 2.2 m, and (c) PW model

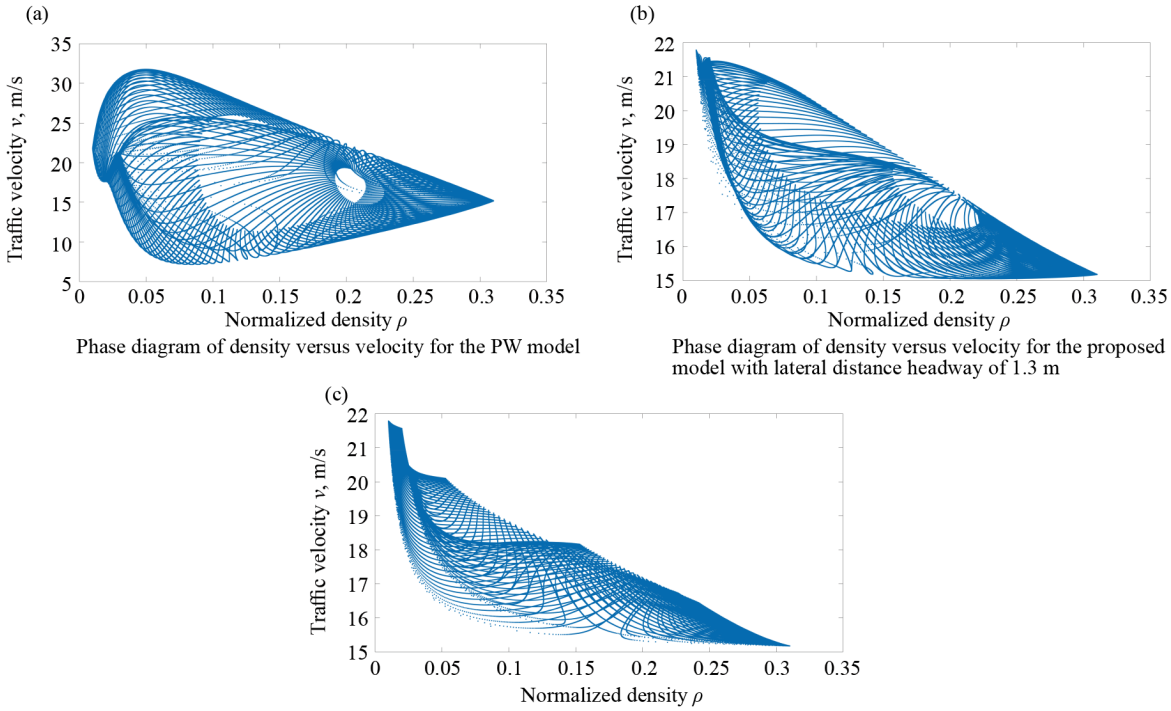

Phase diagram of density versus velocity for the PW model

Phase diagram of density versus velocity for the proposed model with lateral distance headway of 1.3 m

Phase diagram of density versus velocity for the proposed model with lateral distance headway of 2.2 m

Figure 7. Comparison of phase diagram on a circular 3,000 m road: (a) PW model, proposed model with lateral headway of (b) 1.3 m, and (c) 2.2 m

The velocity versus density phase diagram of the proposed model with lateral distance of 1.3 m is shown in Figure 7b. It is demonstrated that the proposed model produces bounded trajectories over a narrow range, and velocitiy stays below the maxium 22 m/s. The narrow range loops over density indicate smoother flow. The downward trend of trajectories, that is, velocity is decreasing as density increases is consistent with the fundamental diagram of traffic flow. While some oscillations are present, they are confined within realistic narrow range, which represents moderate stop and go traffic as observed in the real world traffic. The clustering of trajectories within a narrower than the PW model indicates enhanced stability and a more accurate representation of driver behavior.

It is demonstrated that the proposed model produces more bounded trajectories over a narrow range than with lateral distance headway of 1.3 m as shown in Figure 7b. The velocitiy stays below the maxium 22 m/s. The further narrower range loops over density than as shown in Figure 7b indicate more smoother flow. That is, smaller driver anticipation as shown in Figure 4b than the results shown in Figure 4a causes smoother changes. The overlapped trajectories show that the initial abrupt changes in density reduces and traffic evolves into smooth flow.

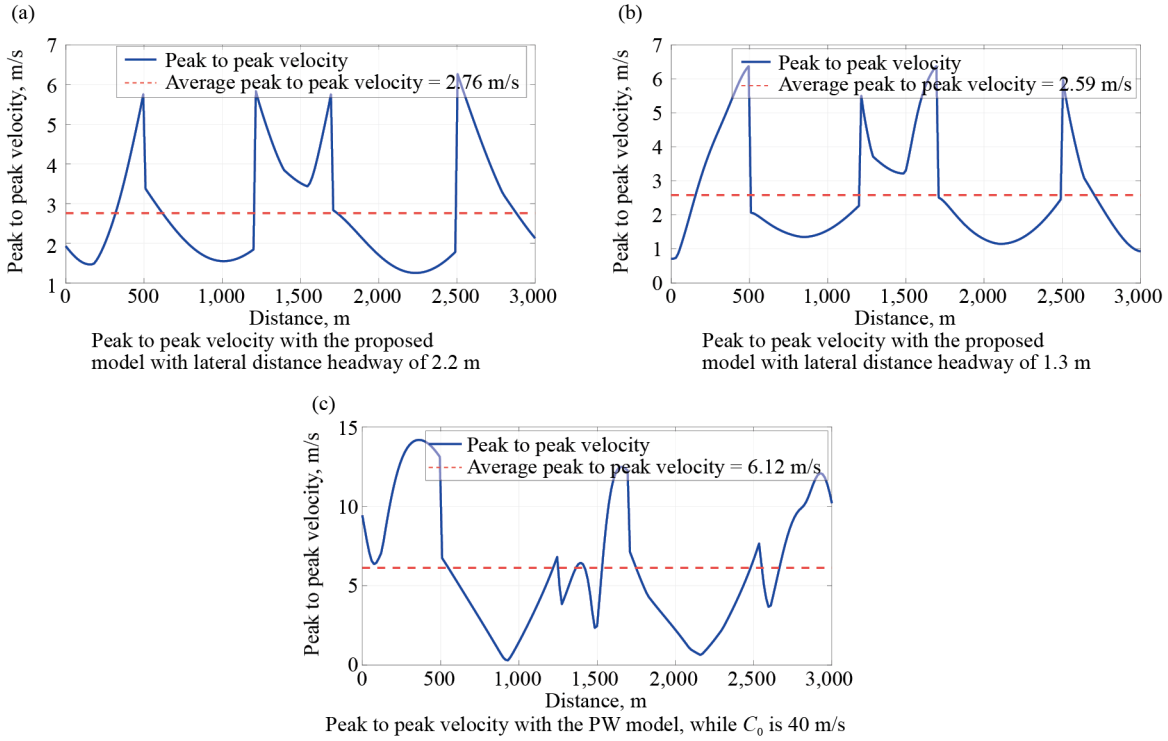

Figure 8. Comparison of peak to peak velocity on a straight 3,000 m road: proposed model with lateral headway of (a) 2.2 m, (b) 1.3 m, and (b) PW model

Figure 8a illustrates the peak to peak velocity obtained with the proposed model over a 3,000 m road with a lateral distance headway of 2.2 m. The peak to peak velocity is 1.49 m/s at 180 m, increases to 5.76 m/s at 495 m, and then decreases to 3.37 m/s at 510 m. It further declines to 1.55 m/s at 1,005 m, before rising slightly to 1.84 m/s at 1,200 m. A significant increase is observed at 1,215 m with a value of 5.84 m/s, followed by a reduction to 3.43 m/s at 1,545 m. At 2,490 m , the velocity is 1.78 m/s, which then peaks at 6.27 m/s at 2,505 m, and finally decreases to 2.13 m/s at 3,000 m. The average peak to peak velocity over the entire 3,000 m is 2.76 m/s.

Figure 8b illustrates the peak to peak velocity obtained with the proposed model over a 3,000 m road with a lateral distance headway of 1.3 m. The peak to peak velocity is 2.96 m/s at 180 m, increases to 6.37 m/s at 495 m, and then decreases to 2.07 m/s at 510 m. It further declines to 1.56 m/s at 1,005 m, before rising slightly to 2.27 m/s at 1,200 m. A significant increase is observed at 1,215 m with a value of 5.04 m/s, followed by a reduction to 3.22 m/s at 1,485 m. At

2,490 m , the velocity is 2.46 m/s, which then peaks at 5.97 m/s at 2,505 m, and finally decreases to 0.93 m/s at 3,000 m. The average peak to peak velocity over the entire 3,000 m is 2.59 m/s.

Figure 8c illustrates the peak to peak velocity obtained with the PW model over a 3,000 m road with C_0 as 40 m/s. The peak to peak velocity is 10.28 m/s at 180 m, increases to 14.18 m/s at 360 m, and then decreases to 6.73 m/s at 510 m. It further declines to 0.30 m/s at 930 m, before rising to 6.84 m/s at 1,245 m. Then it reduces at 1,500 m to 2.46 m/s, followed by an increase to 12.47 m/s at 1,655 m. At 2,490 m, the velocity is 6.40 m/s, which then peaks at 7.65 m/s at 2,535 m, and finally increases to 10.20 m/s at 3,000 m. The average peak to peak velocity over the entire 3,000 m is 6.12 m/s.

The peak to peak velocity of the proposed model as shown in Figures 8a and 8b illustrate that the oscillations are observed in both cases of lateral headway of 2.2 m and 1.3 m, respectively. The larger headway of 2.2 m yields smaller average peak to peak velocity and has smaller velocity variations than with the 1.3 m. However, the maximum peak to peak velocity in both the figures remain below 6.5 m/s, indicating relatively stable traffic flow to the PW model. In contrast, the PW model (Figure 8c) produces considerably larger oscillations, with an average peak to peak velocity of 6.12 m/s and maximum values exceeding 14 m/s. These large variations, such as the rise from 10.28 m/s at 180 m to 14.18 m/s at 360 m, highlight the stronger instability predicted by the PW formulation. The proposed model demonstrates smoother and more damped velocity fluctuations compared to the PW model, suggesting a more realistic representation of traffic flow.

The proposed model reduces the average peak to peak velocity relative to the PW model by 57.7%. This significant reduction in peak to peak velocity by the proposed model produces a smoother traffic flow. And significantly reduces the acceleration/deceleration, which dominantly contributes to fuel consumption and CO_2 emissions. Consequently, the proposed model can be employed for energy efficient and environmentally sustainable traffic operation. This model can improve the passenger comfort level as the traffic oscillations are reduced.

4.3 *Straight road illustration*

The proposed ad PW models performance is compared over a straight road of 3,000 m with a lateral distance headway of 1.3 m. The leading vehicle velocity is 22 m/s. A fine grid with the road step of 1 m is chosen. While the time step is 0.01 s. That is both the models are assessed for the ground truth under the identical conditions. The initial density distribution over the road is

$$\rho_0 = \begin{cases} 0.01, & \text{for } x \leq 1{,}500, \\ \\ 0.4, & \text{for } x \leq 3{,}000. \end{cases} \tag{37}$$

There is no entry of traffic at 0 m, and leaves at 3,000 m, that is the non periodic boundary conditions are employed in the simulations.

Figure 9a illustrates the proposed model velocity behavior over 3,000 m straight road with $\delta x = 1$ m. It is shown that the traffic velocity stays within the maximum 22 m/s and minimum 0 m/s limits, which is an accurate and realistic traffic behavior. The maximum velocity is 18 m/s, while the minimum is 11 m/s.

Figure 9b illustrates the PW model velocity behavior over 3,000 m straight road with $\delta x = 1$ m. It is shown that the traffic velocity goes above and below the maximum 22 m/s and minimum 0 m/s limits. The maximum velocity is 50 m/s and the minimum is -40 m/s, which is an unrealistic and inaccurate behavior.

Based on the illustration of results as shown in Figures 9a and 9b, it is observed that the proposed model velocity stays within the limits and follows the initial density behavior (37). Whereas the PW model velocity behavior dos not within the range and results in negative velocity unrealistically. And does not follow the initial density behavior. Therefore, the proposed is chosen to serve as numerical ground truth and both the models with road step of 8 m (coarse grid) are compared with a fine grid results of the proposed model. Table 2 presents the quantitative comparison between the classical PW model and the proposed model using a coarse-fine grid framework. The Root Mean Square Error (RMSE) for both

velocity and density at 0.1 s, 1 s, 2 s, 4 s, and 10 s is iterated. It is observed that the proposed model has substantially lower velocity RMSE than the PW model. At 0.10 s, the PW model shows a velocity RMSE of 2.09, whereas the proposed model reduces this error to 7.01×10^{-1}, corresponding to an error reduction of approximately 66%. This improvement is more pronounced at 10 s, that is, the PW model velocity RMSE increases to 5.84, while the proposed model remains significantly lower at approximately 1.28. This shows that the PW model gains velocity errors more rapidly due to the nonlinear traffic behavior.

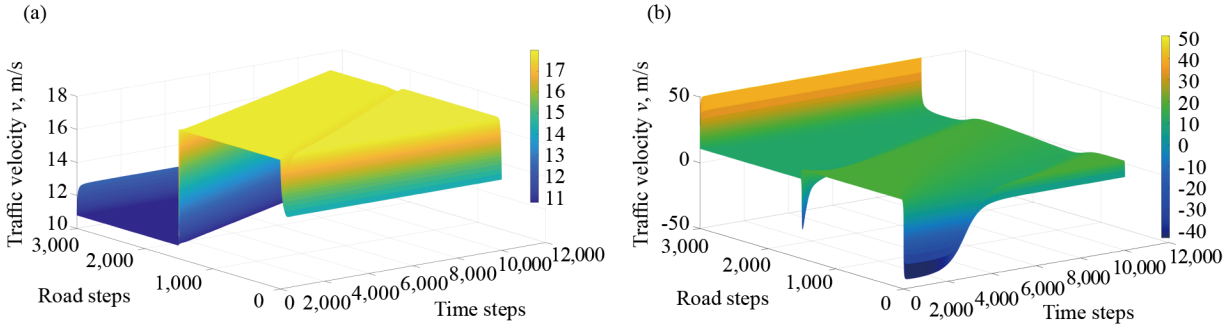

The proposed model velocity behavior on a straight road of 3,000 m on a refined grid of $\delta x = 1$ m

The PW model velocity behavior on a straight road of 3,000 m on a refined grid of $\delta x = 1$ m

Figure 9. Comparison of traffic velocity behavior on a straight 3,000 m road: (a) proposed model and (b) PW model

The density RMSE for both models is of comparable magnitude. That is, the proposed model density RMSE is consistently matching or slightly improving from the PW model. This is an expected behavior, as density behavior is primarily characterized by the traffic conservation principle. Whereas the velocity is more sensitive to the driver anticipation. The comparable density accuracy confirms that the proposed model improves the velocity behavior while the traffic conservation properties are not degraded.

With the increase in time, the difference in RMSE between the proposed and PW models increases and is more prominent for velocity. This highlights that the PW model is more susceptibility to nonphysical and unrealistic oscillations. That is the PW model exhibits large changes in velocity at large and abrupt changes in density. Conversly, the proposed model shows enhanced stability, that is, the proposed driver anticipation term introduces stabilized changes which even better captures the traffic behavior at fine resolution.

Table 2. Velocity, and density error metrics for coarse vs. fine grid

Time (s)	PW model, RMSE(v)	PW model, RMSE(ρ)	Proposed model, RMSE(v)	Proposed model, RMSE(ρ)
0.10	2.09	2.03×10^{-2}	7.01×10^{-1}	2.02×10^{-2}
1.00	5.19	3.95×10^{-2}	8.07×10^{-1}	3.81×10^{-2}
2.00	5.53	4.76×10^{-2}	8.83×10^{-1}	4.50×10^{-2}
4.00	5.62	5.66×10^{-2}	1.03×10^{0}	5.27×10^{-2}
10.00	5.84	6.89×10^{-2}	1.26×10^{0}	6.31×10^{-2}

4.4 *Illustration of longitudnal grade on a straight road*

The proposed models performance is compared over a straight road of 3,000 m with a lateral distance headway of 2.2 m with grades of $\pm 12\%$ and $\pm 1\%$. That is the velocity behavior of the proposed model is analyzed at uphill and downhill longitudnal road grades. The leading vehicle velocity is 22 m/s. The road step is chosen as 8 m, while the time step is 0.01 s. The initial velocity distribution is (37). At 0 m, the velocity is 21.97 m/s at uphill grade of 11%. The velocity

at 504 m reduces to 16.23 m/s, which slightly reduces to 15.80 m/s at 1,200 m. It then reduces to 5.05 m/s at 2,000 m. At 0 m, the velocity is 21.48 m/s at uphill grade of 3%. The velocity at 504 m reduces to 15.75 m/s, which slightly reduces to 15.31 m/s at 1,200 m. It then reduces to 4.58 m/s at 2,000 m. At 0 m, the velocity is 21.11 m/s at downhill grade of −3%. The velocity at 504 m reduces to 15.39 m/s, which slightly reduces to 14.94 m/s at 1,200 m. It then reduces to 4.23 m/s at 2,000 m. At 0 m, the velocity is 20.62 m/s at downhill grade of −11%. The velocity at 504 m reduces to 14.61 m/s, which slightly reduces to 14.45 m/s at 1,200 m. It then reduces to 3.76 m/s at 2,000 m. These results illustrate that increase in the uphill grade increases the resistive gravitational effects, which reduces the velocity. While the downhill grade reduces the gravitational traffic resistance, which results in slight velocity increase. Expectedly, the proposed model can effectively characterize the asymmetric impact of road grades on traffic which highlightes its critical role on speed evolution.

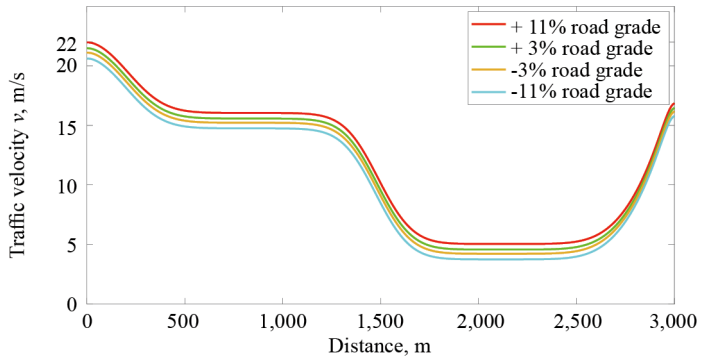

Figure 10. The proposed model velocity behavior on a straight road of 3,000 m on road grades of ± 11% and ± 3%

The results indicate that the PW model induces excessive driver anticipation, producing unrealistic velocity patterns, including values exceeding the maximum limit. Moreover, velocity fluctuations are more pronounced under the PW model compared to the proposed model. In contrast, the proposed model incorporates moderate levels of anticipation and exhibits stable velocity behavior. Realistically, driver anticipation is higher for smaller lateral distance headways than for larger ones. The phase diagram of the PW model is spreaded over a larger range of densities, which exhibits unstable traffic behavior. While with the proposed model, the phase diagram is spreaded over smaller range of densities and has the tendency of smooth flow. The proposed model predicts a safe traffic behavior unlike the PW model. The PW model fails to capture this effect, as it assumes a fixed, non-physical traffic constant uniformly applied across all conditions, which does not reflect real-world dynamics. The proposed model can chracterize the rarefaction and shock waves as shown in Figure 3. By comparison, the proposed model explicitly accounts for the effective angle of vision, vehicle size, forward and lateral distance headways, providing a more realistic representation of driver behavior. Further, the proposed model can effectively characterize the impact of road grades on the traffic as shown in Figure 10.

5. Conclusion

A new macroscopic traffic model is presented that incorporates the effects of effective angle of vision, vehicle size, and forward and lateral distance headways. Unlike the uniform driver anticipation in the PW model, the proposed model adjusts driver anticipation dynamically according to distance headways, with higher anticipation observed at smaller lateral headways, as expected. The model realistically captures both large changes (shock waves) and small changes (rarefaction) in traffic, while keeping velocity and density within defined limits, thereby predicting stable traffic flow. In contrast, the PW model produces more oscillatory velocity patterns and wider velocity-density trajectories, leading to congested and less realistic traffic predictions. With the proposed model, trajectories remain within a smaller range, and larger lateral headways promote smoother traffic flow. The findings indicate that this approach captures traffic behavior more accurately and

reliably under diverse conditions, making it ideal for traffic control planning and enhancing autonomous vehicle operation. Further, the proposed model can effectively characterize the road grade impact. Based on the findings, the proposed model has the strong potential for energy-aware traffic control, eco-driving strategies, and sustainable transportation system design.

The study in this paper is based on the theoretical and bench mark on a fine-coarse grid due to the scarcity of high-resolution spatiotemporal datasets [65]. Future improvement to the proposed will integrate high resolution datasets and AI-driven calibration techniques to perform the real world validation and deployment.

Conflict of interest

The authors declare no competing financial interest.

References

[1] Lauren P. Evaluating macroscopic traffic flow models using real vehicle trajectory data. *Journal of High School Science*. 2025; 9(1): 52–73. Available from: https://doi.org/10.64336/001c.128562.

[2] Luo Y, Chen Y, Lu K, Chen L, Zhang J. Modeling and analysis of heterogeneous traffic flow considering dynamic information flow topology and driving behavioral characteristics. *Physica A: Statistical Mechanics and Its Applications*. 2024; 637: 129521. Available from: https://doi.org/10.1016/j.physa.2024.129521.

[3] Liu C, Wang Z, Nacpil EJC, Hou W, Zheng R. Analysis of visual risk perception model for braking control behaviour of human drivers: A literature review. *IET Intelligent Transportation Systems*. 2022; 16(6): 711–841. Available from: https://doi.org/10.1049/itr2.12170.

[4] Hoffmann ER, Mortimer RG. Scaling of relative velocity between vehicles. *Accident Analysis and Prevention*. 1996; 28(4): 415–421. Available from: https://doi.org/10.1016/0001-4575(96)00005-X.

[5] Saifuzzaman M, Zheng Z. Human factors affecting the behavior of drivers during car-following: A literature review. *Transportation Research Part C: Emerging Technologies*. 2014; 48: 379–403. Available from: https://doi.org/10.1016/j.trc.2014.09.008.

[6] Nemchinov D, Martiyahin D, Mikhailov A, Kostsov A, Nemchinov M. Research of accepted headways and visibility conditions on intersections. *Transportation Research Procedia*. 2020; 45: 13–20. Available from: https://doi.org/10.1016/j.trpro.2020.02.057.

[7] Narayanan S, Palraj S, Mani M, Pathak S. Automotive vision and obstruction assessment for driver. In: *SAE Technical Paper*. Warrendale, PA, USA: SAE International; 2017. p.1–8.

[8] Treiber M, Hennecke A, Helbing D. Congested traffic states in empirical observations and microscopic simulations. *Physical Review E*. 2000; 62(2): 1805. Available from: https://doi.org/10.1103/PhysRevE.62.1805.

[9] Brackstone M, McDonald M. Car-following: A historical review. *Transportation Research Part F: Traffic Psychology and Behaviour*. 1999; 2(4): 181–196. Available from: https://doi.org/10.1016/S1369-8478(00)00005-X.

[10] Ahmed KI. *Modeling drivers' acceleration and lane changing behavior*. Doctoral Dissertation. Cambridge, MA, USA: Massachusetts Institute of Technology; 1999.

[11] Kesting A, Treiber M, Helbing D. General lane-changing model MOBIL for car-following models. *Transportation Research Record*. 2007; 1999(1): 86–94. Available from: https://doi.org/10.3141/1999-10.

[12] Federal Highway Administration. *Weather Related Crash Statistics*. 2020. Available from: https://ops.fhwa.dot.gov/weather/q1_roadimpact.htm [Accessed 27th June 2025].

[13] Keimer A, Pflug L. Nonlocal balance laws-an overview over recent results. In: *Handbook of Numerical Analysis*. Amsterdam, Netherlands: Elsevier; 2023. p.183–216.

[14] Peng Y, Abdel-Aty M, Shi Q, Yu R. Assessing the impact of reduced visibility on traffic crash risk using microscopic data and surrogate safety measures. *Transportation Research Part C: Emerging Technologies*. 2017; 74: 295–405. Available from: https://doi.org/10.1016/j.trc.2016.11.022.

[15] Ni R, Kang JJ, Andersen GJ. Age related declines in car following performance under simulated fog conditions. *Accident Analysis and Prevention*. 2010; 42(3): 818–826. Available from: https://doi.org/10.1016/j.aap.2009.04.023.

[16] Rosey F, Aillerie I, Espie S, Vienne F. Driver behaviour in fog is not only a question of degraded visibility-a simulator study. *Safety Science*. 2007; 95: 50–61. Available from: https://doi.org/10.1016/j.ssci.2017.02.004.
[17] Portland Bureau of Transportation. *Vehicle Size Trends and Safety*. 2025. Available from: https://www.portland.gov/transportation/vision-zero/vehicle-size-trends-and-safety [Accessed 24th August 2025].
[18] Biswas RK, Friswell R, Olivier J, Williamson A, Senserrick T. A systematic review of definitions of motor vehicle headways in driver behaviour and performance studies. *Transportation Research Part F: Traffic Psychology and Behaviour*. 2021; 77: 38–54. Available from: https://doi.org/10.1016/j.trf.2020.12.011.
[19] Khan ZH, Imran W, Gulliver TA, Khattak KS, Din GU, Minallah N, et al. Macroscopic traffic characterization based on driver memory and traffic stimuli. *Transportation Engineering*. 2023; 14: 100208. Available from: https://doi.org/10.1016/j.treng.2023.100208.
[20] Zhang Y, Yang X. Discrete macroscopic traffic flow model considering the lane-changing behaviors in the mixed traffic environment. *Transportation Research Part C: Emerging Technologies*. 2024; 164: 104672. Available from: https://doi.org/10.1016/j.trc.2024.104672.
[21] Imran W, Pariota L. Macroscopic evaluation of traffic flow in view of connected and autonomous vehicles: A simulation-based approach. *Alexandria Engineering Journal*. 2023; 79: 581–590. Available from: https://doi.org/10.1016/j.aej.2023.08.034.
[22] Rowan D, He H, Hui F, Yasir A, Mohammed Q. A systematic review of machine learning-based microscopic traffic flow models and simulations. *Communications in Transportation Research*. 2025; 5: 100164. Available from: https://doi.org/10.1016/j.commtr.2025.100164.
[23] Lighthill MJ, Whitham GB. On kinematic waves II. A theory of traffic flow on long crowded roads. *Proceedings of the Royal Society of London Series A: Mathematical and Physical Sciences*. 1955; 229(1178): 317–345. Available from: https://doi.org/10.1098/rspa.1955.0089.
[24] Richards PI. Shock waves on the highway. *Operations Research*. 1956; 4(1): 42–51.
[25] Iftikhar A, Khan ZH, Gulliver TA, Khattak KS, Ahmed I. Macroscopic traffic characterization based on distance headway. *Civil Engineering Journal*. 2024; 10(12): 4058–4068. Available from: https://doi.org/10.28991/CEJ-2024-010-12-016.
[26] Daganzo C. Requiem for second-order fluid approximations of traffic flow. *Transportation Research Part B: Methodological*. 1995; 29(4): 277–286. Available from: https://doi.org/10.1016/0191-2615(95)00007-Z.
[27] Maerivoet S, De Moor B. *Transportation Planning and Traffic Flow Models*. Leuven: Katholieke Universiteit Leuven; 2008.
[28] Liu G, Lyrintzis A, Michalopoulos P. Improved high-order model for freeway traffic flow. *Transportation Research Record*. 1998; 1644(1): 37–46. Available from: https://doi.org/10.3141/1644-05.
[29] Khan ZH, Khattak KS, Gulliver TA. Impact of driver anticipation on traffic at a ramp in foggy conditions. *Mathematics*. 2025; 13: 2855. Available from: https://doi.org/10.3390/math13172855.
[30] Firat T, Eroglu D. Data-driven modeling of traffic flow in macroscopic network systems. *Chaos*. 2025; 35: 093134. Available from: https://doi.org/10.1063/5.0285930.
[31] Jiang R, Wu Q, Zhu Z. A new continuum model for traffic flow and numerical tests. *Transportation Research Part B: Methodological*. 2002; 36(5): 405–419. Available from: https://doi.org/10.1016/S0191-2615(01)00010-8.
[32] Bonzani I, Mussone L. On the derivation of the velocity and fundamental traffic flow diagram from the modelling of the vehicle-driver behaviors. *Mathematical and Computer Modelling*. 2009; 50(7–8): 1107–1112. Available from: https://doi.org/10.1016/j.mcm.2009.06.004.
[33] Greenberg H. An analysis of traffic flow. *Operations Research*. 1959; 7(1): 79–85.
[34] Salter RJ. The relationship between speed, flow and density of a highway traffic stream. In: *Highway Traffic Analysis and Design*. London: Palgrave; 1996. p.119–130.
[35] Khan ZH, Gulliver TA. A macroscopic traffic model based on transition velocities. *Journal of Computational Science*. 2020; 43: 101131. Available from: https://doi.org/10.1016/j.jocs.2020.101131.
[36] Zhang H. A theory of non-equilibrium traffic flow. *Transportation Research Part B: Methodological*. 1998; 32(7): 485–498. Available from: https://doi.org/10.1016/S0191-2615(98)00014-9.
[37] Payne HJ. Models of freeway traffic and control. In: *Mathematical Models of Public Systems (Simulation Council Proceedings)*. La Jolla, CA: Simulation Councils, Inc.; 1971. p.51–61.
[38] Whitham GB. *Linear and Nonlinear Waves*. New York: Wiley; 1971.

[39] Kühne RD, Rödiger MB. Macroscopic simulation model for freeway traffic with jams and stop-start waves. In: *Proceedings of the Winter Simulation Conference*. Phoenix, AZ, USA: IEEE; 1991. p.762–770.
[40] Kerner BS, Konhäuser P. Cluster effect in initially homogeneous traffic flow. *Physical Review E*. 1993; 48(4): R2335. Available from: https://doi.org/10.1103/PhysRevE.48.R2335.
[41] Papageorgiou M, Blosseville JM, Hadj-Salem H. Macroscopic modelling of traffic flow on the boulevard peripherique in Paris. *Transportation Research Part B: Methodological*. 1989; 23(1): 29–47. Available from: https://doi.org/10.1016/0191-2615(89)90021-0.
[42] Wu L, Sun Z, Liu J, Shan D, Ma X, Zhu T. Unveiling the impact of heterogeneous driving behaviors on traffic flow: A mesoscale multi-agent modeling approach. *Computers and Electrical Engineering*. 2024; 119: 109500. Available from: https://doi.org/10.1016/j.compeleceng.2024.109500.
[43] Burger R, Munoz C, Mandiola ST. Interaction of jamitons in second-order macroscopic traffic models. *Nonlinearity*. 2025; 38(9): 095001. Available from: https://doi.org/10.1088/1361-6544/adfa60.
[44] Del Castillo J, Pintado P, Benitez F. The reaction time of drivers and the stability of traffic flow. *Transportation Research Part B: Methodological*. 1994; 28(1): 35–60. Available from: https://doi.org/10.1016/0191-2615(94)90030-2.
[45] Aw A, Rascle M. Resurrection of "second order" models of traffic flow. *SIAM Journal on Applied Mathematics*. 2000; 60(3): 916–938. Available from: https://doi.org/10.1137/S0036139997332099.
[46] Morgan JV. *Numerical methods for macroscopic traffic models*. Doctoral Dissertation. Berkshire: University of Reading; 2002.
[47] Berg P, Mason A, Woods A. Continuum approach to car-following models. *Physical Review E*. 2000; 61: 1056–1066. Available from: https://doi.org/10.1103/PhysRevE.61.1056.
[48] Kerner BS, Konhäuser P. Structure and parameters of clusters in traffic flow. *Physical Review E*. 1994; 50: 54–83. Available from: https://doi.org/10.1103/physreve.50.54.
[49] Jiang R, Wu QS, Zhu ZJ. A new continuum model for traffic flow and numerical tests. *Transportation Research Part B: Methodological*. 2002; 36(5): 405–419. Available from: https://doi.org/10.1016/S0191-2615(01)00010-8.
[50] Qaiser T, Altamimi AB, Khan FA, Alsaffar M, Alreshidi A, Khattak KS, et al. A new macroscopic traffic flow characterization incorporating traffic emissions. *Applied Sciences*. 2023; 13(9): 5545. Available from: https://doi.org/10.3390/app13095545.
[51] Yu C, Zhang J, Yao D, Zhang R, Jin H. Speed-density model of interrupted traffic flow based on coil data. *Mobile Information Systems*. 2016; 2016(1): 7968108. Available from: https://doi.org/10.1155/2016/7968108.
[52] Treiber M, Kesting A. *Traffic Flow Dynamics: Data, Models and Simulation*. Cham: Springer; 2025.
[53] Toro EF. *Riemann Solvers and Numerical Methods for Fluid Dynamics: A Practical Introduction*. Berlin: Springer; 2011.
[54] Khan ZH, Imran W, Azeem S, Khattak KS, Gulliver TA, Aslam MS. A macroscopic traffic model based on driver reaction and traffic stimuli. *Applied Sciences*. 2019; 9(14): 2848. Available from: https://doi.org/10.3390/app9142848.
[55] Corli A, Fan H. String stability in traffic flows. *Applied Mathematics and Computation*. 2023; 443: 127775. Available from: https://doi.org/10.1016/j.amc.2022.127775.
[56] Toro EF, Hidalgo A, Dumbser M. Force schemes on unstructured meshes I: Conservative hyperbolic systems. *Journal of Computational Physics*. 2009; 228(9): 3368–3389. Available from: https://doi.org/10.1016/j.jcp.2009.01.025.
[57] Kachroo PPE, Wadoo SA, Al-nasur SJ, Shende A. Numerical methods. In: *Pedestrian Dynamics Feedback Control of Crowd Evacuation*. New York: Springer; 2008. p.61–93.
[58] de Moura CA, Kubrusly CS. *The Courant-Friedrichs-Lewy (CFL) Condition: 80 Years After Its Discovery*. Berlin: Springer; 2013.
[59] CarRoar. *Average Vehicle Length*. 2026. Available from: https://carroar.com/car-length/ [Accessed 24th January 2026].
[60] Roads General Authority. *Saudi Highway Code (SHC 301): Highway Geometric Design*. 2024. Available from: https://shc.rga.gov.sa [Accessed 20th January 2026].
[61] Li X, Wang W, Roetting M, Gong J. Effects of lateral clearance on driving behavior and safety. *Accident Analysis and Prevention*. 2021; 152: 105995.
[62] Helbing D. Traffic and related self-driven many-particle systems. *Reviews of Modern Physics*. 2001; 73(4): 1067–1141. Available from: https://doi.org/10.1103/RevModPhys.73.1067.

[63] Basak K, Hetu SN, Zheminli, Azevedo CL, Loganathan H, Toledo T, et al. Modeling reaction time within a traffic simulation model. In: *Proceedings of the IEEE International Conference on Intelligent Transportation Systems*. The Hague, Netherlands: IEEE; 2013. p.302–309.

[64] Yi P, Lu J, Zhang Y, Lu H. Safety-based capacity analysis for Chinese highways. *IATSS Research*. 2004; 28(1): 47–55. Available from: https://doi.org/10.1016/S0386-1112(14)60091-1.

[65] Yao Z, Xu T, Jiang Y, Hu R. Linear stability analysis of heterogeneous traffic flow considering degradations of connected automated vehicles and reaction time. *Physica A: Statistical Mechanics and Its Applications*. 2021; 561: 125218. Available from: https://doi.org/10.1016/j.physa.2020.125218.